Quaternary International 513 (2019) 1–7

Contents lists available at ScienceDirect

Quaternary International

journal homepage: www.elsevier.com/locate/quaint

# Holocene climate dynamics derived from pollen record of Jiulongchi wetland in Fanjing Mountain, southwest China

Yang Gao[a], Kangning Xiong[a,*], Mingying Quan[a], Bing Song[b], Haijun Peng[c], Huirong Peng[a], Weidan Shen[a], Kunshan Bao[b,**]

[a] School of Karst Science, Guizhou Normal University/ State Key Laboratory Incubation Base for Karst Mountain Ecology Environment of Guizhou Province, Guiyang, 550001, China
[b] State Key Laboratory of Lake Science and Environment, Nanjing Institute of Geography and Limnology, Chinese Academy of Sciences, Nanjing, 210008, China
[c] State Key Laboratory of Environmental Geochemistry, Institute of Geochemistry, Chinese Academy of Sciences, Guiyang, 550081, China

ARTICLE INFO

*Keywords:*
Holocene
Climate change
Pollen
EASM
Alpine wetland

ABSTRACT

An alpine wetland core was obtained to a depth of 4.0 m from the Fanjing Mountain in southwest China. Sections of the core were dated with $^{14}C$ data obtained with high resolution mass spectrometry (AMS), and Holocene climate changes were inferred by categorizing predominant tree and fern vegetation identified from pollen and spore counts at various core depths. The temperature increased during 11.9–8.0 cal ka BP, and the warmest period was during 8.0–4.6 cal ka BP. Then, it gradually became cooler during the late Holocene. Our temperature estimates were in good agreement with the previous studies of the Holocene temperature in the Asian monsoon areas. There were two relatively wet periods of 10.7–8.0 cal ka BP and 4.6–2.6 cal ka BP. There was an asynchronous precipitation trend in the south, north and southwest China, which was probably due to the different monsoon impacts. In East Asian summer monsoon (EASM) area, the monsoon precipitation gradually transgressed northward during the early to middle Holocene and regressed southward during the late Holocene. Our results will be useful to improve the understanding of the coherent spatio-temporal patterns of climate evolution in EASM region in China.

## 1. Introduction

East Asian monsoon (EAM) climate system transports heat and water vapor from the Pacific and Indian Oceans to the Asian continent and thus controls air temperature, precipitation amount and vegetation development (Zhou et al., 2016). Recently, a large number of palaeo-environmental records have been used to understand the Holocene climate change in the east EAM areas in China (Chen et al., 2014; Dykoski et al., 2005; Mackenzie et al., 2018; Shen et al., 2006; Song et al., 2012; Stebich et al., 2015; Wang et al., 2005; Xiao et al., 2014; Yang et al., 2016). However, the Holocene climate change history as reconstructed from different regions shows spatio-temporal variability and different control mechanisms of the Asian monsoon (Wang et al., 2010). In southwest China (i.e., Tibetan Plateau and Yunnan Province), the cold and dry climate gradually transitioned to warm and wet condition during the early to middle Holocene, and afterwards, reverted to cold and dry climate (Xiao et al., 2014; Yang et al., 2016). The warm and humid climate indicates strong Indian summer monsoon (ISM), and the cold and dry climate denotes weak ISM (Xiao et al., 2014; Yang et al., 2016). In the north China, Holocene climate changes as shown by the geological records were very similar to the southwest China and the impact by East Asian summer monsoon (EASM) was weak (Chen et al., 2014). In northeast China, the Holocene precipitation trend derived from pollen records reached a maximum at approximately 4000 cal a before present (BP), and decreased afterwards (Stebich et al., 2015). In the south China, there are debates about the Holocene climate dynamics, their variation history and the main control factors of ISM or EASM (Jia et al., 2015; Sheng et al., 2017; Wu et al., 2012). With respect to the timing of the Holocene Optimum (HO) in the EAM region, there is a time-regression hypothesis that EASM maximum retreated southeastward because of weakening of summer insolation throughout the Holocene (An et al., 2000; Zhou et al., 2016). However, Ran and Feng (2013) pointed out that the strength of EASM had gradually transgressed northward in the early Holocene and then gradually regressed southward in the late Holocene. Therefore, more high-resolution Holocene climatic records are needed in south China to better

* Corresponding author.
** Corresponding author.
*E-mail addresses:* xiongkn@163.com (K. Xiong), ksbao@niglas.ac.cn (K. Bao).

https://doi.org/10.1016/j.quaint.2019.01.009
Received 4 October 2018; Received in revised form 7 January 2019; Accepted 7 January 2019
Available online 08 January 2019
1040-6182/ 

understand the mechanisms controlling the spatio-temporal variability of the EAM in China.

In this study, we conducted a high-resolution palynological analysis for an accelerator mass spectrometry (AMS) carbon 14 ($^{14}$C) dated sedimentary core from Jiulongchi wetland in Fanjing Mountain, located in southwest China. Our objectives are to reconstruct the history of Holocene climate dynamics and to understand the spatio-temporal patterns of climate evolution in EASM region in China. Holocene precipitation asynchronous among south, southwest and north of China is also generally discussed.

## 2. Geological setting

Fanjing Mountain (27º49′50"-28º01′30" N, 108º45′55"-108º48′30" E) lies in northeastern Guizhou province, the transitional zone from the Yunnan-Guizhou Plateau towards the Western Hunan Hills. It is located the center of subtropical region in China, and is characterized by the humid subtropical monsoon climate in mountain area. The average annual temperature is about 6–17 °C. The coldest and hottest month is January and July, with an average of 3.1–5.1 °C and 15–27 °C, respectively. The annual precipitation is about 1100–2600 mm. In this region, the Precambrian strata had been well preserved and widely distributed, including Fanjingshan Group (ca. 270 km$^2$), and the Neoproterozoic Banxi Group (Su et al., 2014). The elevation of its peak is about 2572 m and the foot of the mountain is about 500 m. The vertical zonal vegetation were divided into five zones, including evergreen broadleaf forest (0–1300 m), mixed evergreen and deciduous broadleaf forest (1300–1900 m), deciduous broadleaf forest (1900–2100 m), coniferous forest (2100–2400 m) and meadow (2400–2572 m). It provided important shelters for many relict, endemic and endangered plant species (i.e., *Paulownia kawakamii*, *Bretschneidera sinensis*) and animal species (i.e., *Andrias davidianus*, *Moschus berezovskii*).

## 3. Materials and methods

### 3.1. Sample collection

We collected a 4 m sediment core (marked as JL15) in October 2015 by a Russian peat sampler (6 cm in diameter) from Jiulongchi wetland at Fanjing Mountain, Guizhou province of China (Fig. 1). The location is 108º41′33.05"E and 27º53′57.82" N with an altitude of 2048 m above the sea level. This site is generally located at the broad-leaved deciduous forest zone. The core was sectioned on site at 5 cm intervals into 80 samples. The sediments were mainly composed of clay. The colors changed from light to dark with increasing depth. The water contents were all higher than 40%, and decreased with increasing depth.

### 3.2. Palynological analysis

Sample aliquots (1.4–2.5 g) were dried at 105 °C overnight and then subjected to hydrochloric acid (15%, HCl) and hydrofluoric acid (45%, HF) digestion for subsequent palynological analysis according to the general procedure outlined by (Faegri and Iversen, 1989). After mixed-acid digestion, the slury was sieved through a 7-μm mesh to remove small particles. *Lycopodium* spores were added to each sample to calculate the pollen concentrations. The pollen and spores were identified using a LEICA (DMR) microscope at 400 × magnification. All sample counting was completed using at least two slides and generally, the pollen counts exceeded 300 grains. The arboreal pollen/total pollen (AP/T) ratio was calculated to simplify the interpretation of pollen records. Pollen diagrams and assemblage zone boundaries were drawn using stratigraphically constrained cluster analysis (CONISS) with the Tilia 1.7.16 software package (Grimm, 2011).

### 3.3. AMS $^{14}$C dating and calibration

We chose nine bulk organic matter samples at different depths in the core and sent them to the Beta Analytic Testing Lab (Miami, Florida, USA) for AMS $^{14}$C age determination (Table 1). The Clam 2.0.1 software was used to calibrate all radiocarbon ages (Blaauw, 2010). Radiocarbon ages were calibrated using the INTAL13 tree-ring dataset (Reimer et al., 2013).

### 3.4. Statistical analysis

The pollen types including 102 pollen taxa from the JL15 core were subjected to principle component analysis (PCA) to obtain the variation trends in pollen sequences by extracting the main information of environmental change following the method of Etienne et al. (2013) and Xu et al. (2013). Two main factors were selected according to the score ranking. Based on the eigenvalue difference of X/Y axis and the ecological characteristics of pollen taxa, the environmental information reflected by the two axes could be inferred and interpreted, respectively.

## 4. Results

### 4.1. Stratigraphy and chronology

In the Jiulongchi wetland, the sedimentary environment was relatively stable during the Holocene, with the similar sediments of silty clay (Fig. 2). The nine AMS $^{14}$C dates were used as chronological control for the palynological spectrum (Table 1). Based on the calm 2.0.1 software, we calculated the ages of climate change points and sedimentation rates (Fig. 2), without considering sediment compaction effects. The sedimentation rate fluctuated from 7.4 to 166.7 cm ka$^{-1}$. The lowest was (9.9 cm ka$^{-1}$) and the range was between 0 and 25 cm (ca. 0–2572 cal a BP). The sedimentation rates were 43.9 cm ka$^{-1}$ and 82.9 cm ka$^{-1}$ in the periods of 4635–2572 cal a BP and 10699-7996 cal a BP, respectively. The highest value was (165.13 cm ka$^{-1}$) occurring between 325 and 355 cm depths (ca. 10517-10699 cal a BP).

### 4.2. Pollen data

Totally 102 pollen types were identified in the core JL15 samples, including 70 arboreal taxa, 25 herbaceous taxa and 7 fern taxa. The main results of the analysis are presented in simplified pollen diagrams (Fig. 3). According to the relationship between the parent plant and biotope, the palynomorph included four groups: conifer arboreal pollen (AP), broadleaf AP, non-arboreal pollen (NAP), and fern spores. Based on CONISS analysis, the identified pollen assemblage could be divided into five major zones (Fig. 3).

Zone I (398–355.5 cm, 11.9–10.7 cal ka BP) revealed predominance of broadleaf AP taxa (69.1%) with *Cyclobalanopsis* (32.3%) and *Carpinus* (7.5%). The conifer AP was about 4.7% and the herb pollen was about 12.1%. The fern spores accounted for 14.0% in which *Polypodiaceae* (12.6%) was predominant.

Zone II (355.5–175.5 cm, 10.7–8.0 cal ka BP) revealed predominance of broadleaf AP taxa (82.9%) with *Cyclobalanopsis* (48.6%) and *Carpinus* (6.0%). The conifer AP decreased to 3.6% and the herb pollen decreased to 5.1%. The fern spores were 8.4% in which *Polypodiaceae* (7.8%) was predominant.

Zone III (175.5–108.5 cm, 8.0–4.6 cal ka BP) revealed predominance of broadleaf AP taxa (87.5%) with *Cyclobalanopsis* (53.6%) and *Carpinus* (5.2%). The conifer AP decreased to 2.9% and the herb pollen was 5.1%. The fern spores were 8.4% in which *Polypodiaceae* (5.9%) was predominant.

Zone IV (108.5–18.5 cm, 4.6–2.6 cal ka BP) revealed predominance of broadleaf AP taxa (82.9%) with *Cyclobalanopsis* (50.4%) and *Carpinus* (5.7%). The conifer AP was 3.6% and the herb pollen increased to 8.4%.

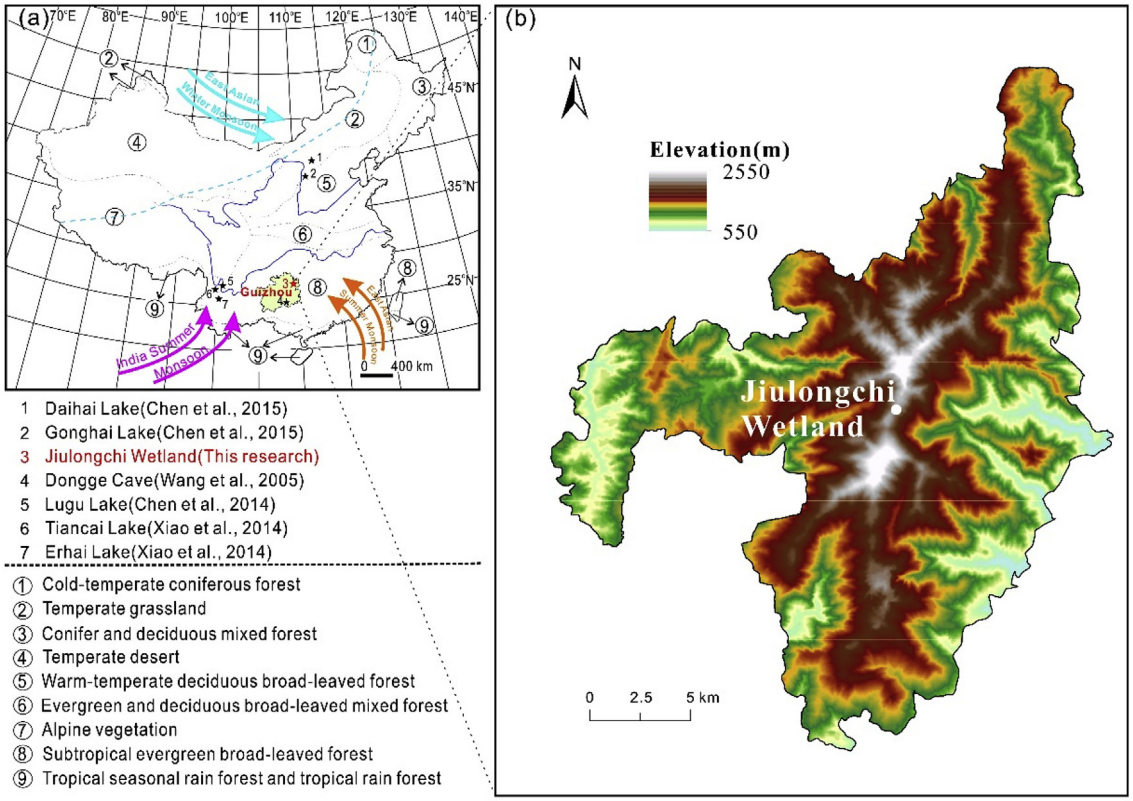


**Fig. 1.** Location of the sampling site at Jiulongchi wetland in Fanjing Mountain, SW China (a) and the topographic map of Fanjing Mountain (b).

**Table 1**
AMS$^{14}$C dates for the core JL15 from Jiulongchi wetland in Guizhou Province, SW China.

| Depth (cm) | Materials | $\delta^{13}$C (‰) | $^{14}$C age (a BP) | Calibration (a BP) | Probability (%) | Code No. |
|---|---|---|---|---|---|---|
| 2.5 | organic | −25.3 | 370 ± 30 | 425 ± 111 | 95 | Beta-452781 |
| 27.5 | organic | −26.2 | 2570 ± 30 | 2815 ± 79 | 95 | Beta-438337 |
| 57.5 | organic | −27.6 | 4010 ± 30 | / | / | Beta-452782 |
| 102.5 | organic | −28.4 | 3680 ± 30 | 4520 ± 109 | 89.4 | Beta-438338 |
| 177.5 | organic | −28.9 | 6370 ± 30 | 8107 ± 90 | 95 | Beta-452783 |
| 242.5 | organic | −30.0 | 7610 ± 30 | 9454 ± 24 | 95 | Beta-438339 |
| 317.5 | organic | −28.7 | 8280 ± 30 | 10472 ± 208 | 95 | Beta-452784 |
| 357.5 | organic | −28.5 | 8430 ± 30 | 10711 ± 54 | 93.4 | Beta-438340 |
| 397.5 | organic | −25.9 | 9040 ± 30 | 11941 ± 118 | 95 | Beta-452785 |

The fern spores were 5.1% in which *Polypodiaceae* (5.3%) was predominant.

Zone V (18.5–0 cm, 2.6 cal ka BP− present) revealed predominance of broadleaf AP taxa (69.1%) with *Cyclobalanopsis* (32.1%). The conifer AP was 4.7% with *Pinus* (8.8%). The herb pollen increased to 12.1%. The fern spores increased to 14% with *Polypodiaceae* (9.9%) being dominant.

### 4.3. PCA of pollen data

The PCA biplots for the main pollen types are shown in Fig. 4. In the first principal component, the eigenvalues of axis 1 was 0.73. However, the eigenvalue of axis 2 was only 0.06 (Fig. 4). The AP pollen of *Pinus*, *Carpinus* (broadleaf deciduous), *Fagus* (temperate deciduous), and *Quercus* (temperate evergreen), as well as the NAP pollen of *Artemisia*, *Cyperaceae*, *Poaceae*, and *Polypodiaceae* were in the positive direction. The AP pollen of *Cyclobalanopsis* (tropical to subtropical) was in the negative direction. In this case, the negative score indicates a warmer climate, whereas the positive score denotes a cooler climate.

## 5. Discussion

### 5.1. Climate change inferred from the pollen record

The AP/T ratio has been recognized as one of the important cool/warm proxies (Park et al., 2016; Zhou et al., 2016). It has similar trend with the F1 score in this study, which revealed a detailed Holocene history of vegetation and climate change in this area (Fig. 5).

During 11.9–10.7 cal ka BP (Zone I), the percentages of subtropical AP and subtropical to tropical AP were 33.5% and 11.9%, respectively. The proxies of AP/T and F1 score were 8.6 and 1.5, respectively. They suggested a relatively cooler climate. In this period, the herb and fern spores mainly consisted of *Cyperaceae*, *Poaceae* and *Polypodiaceae*, which suggested a wetland or relatively wet terrestrial environment at that time (Panigrahi and Patnaik, 1961; Yang et al., 2016). The nearby records in Tiancai Lake, Erhai Lake and Lugu Lake in Yunnan Province, southwestern China (Fig. 1) (Shen et al., 2006; Xiao et al., 2014) also indicated a cold and dry climate in this period. Therefore, the Jiulongchi lake would start to transition to a wetland environment at that time due to the cool and dry climate.

During 10.7–8.0 cal ka BP (Zone II), the percentage of subtropical

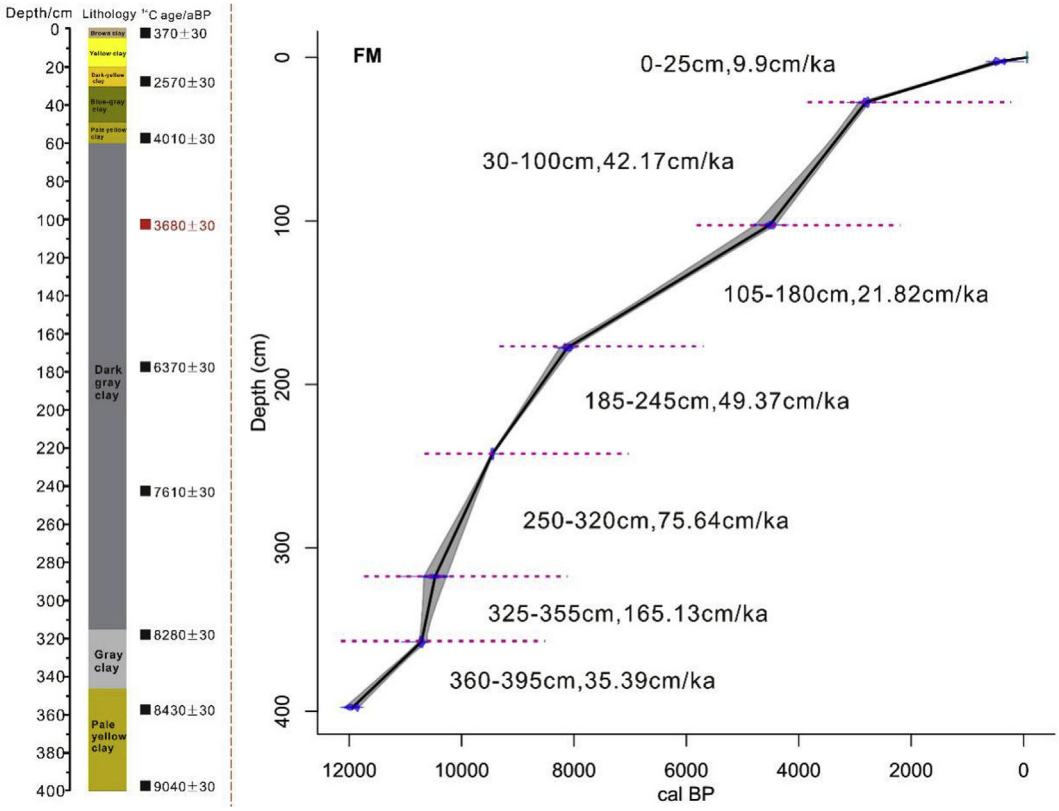


**Fig. 2.** Schematic diagram of lithologic variation and Bayesian age-depth model for core JL15 from Jiulongchi wetland in Guizhou Province, SW China.

AP and subtropical to tropical AP increased to 49.7% and 13.6%, respectively, and the conifer AP and temperate AP showed a decreasing trend compared to the earlier period. The proxies of AP/T and F1 score were 9.4 and −0.1, respectively. Such variations of the spectrum would suggest a warmer climate. In this period, the percentage of herb and fern spores decreased. The pollen concentration and sedimentation rates were relatively high, $109.5 \times 10^3$ grains/g and 82.9 cm $ka^{-1}$, respectively. These would be due to a wetter climate than the earlier period. In a separate investigation adjacent to our study area, a palynological record from Tiancai lake (Fig. 1) showed that the *Betula* pollen content gradually decreased, the deciduous *Quercus* and *Tsuga* pollens increased, and the treeline continued to rise in the early Holocene (Xiao et al., 2014). Another nearby lake sediment (Qinghai crater lake) also revealed a decrease for the drought-resistant herbaceous components and an expansion of the evergreen broadleaved forest in this period (Xiao et al., 2014). Meanwhile, the pollen evidence from

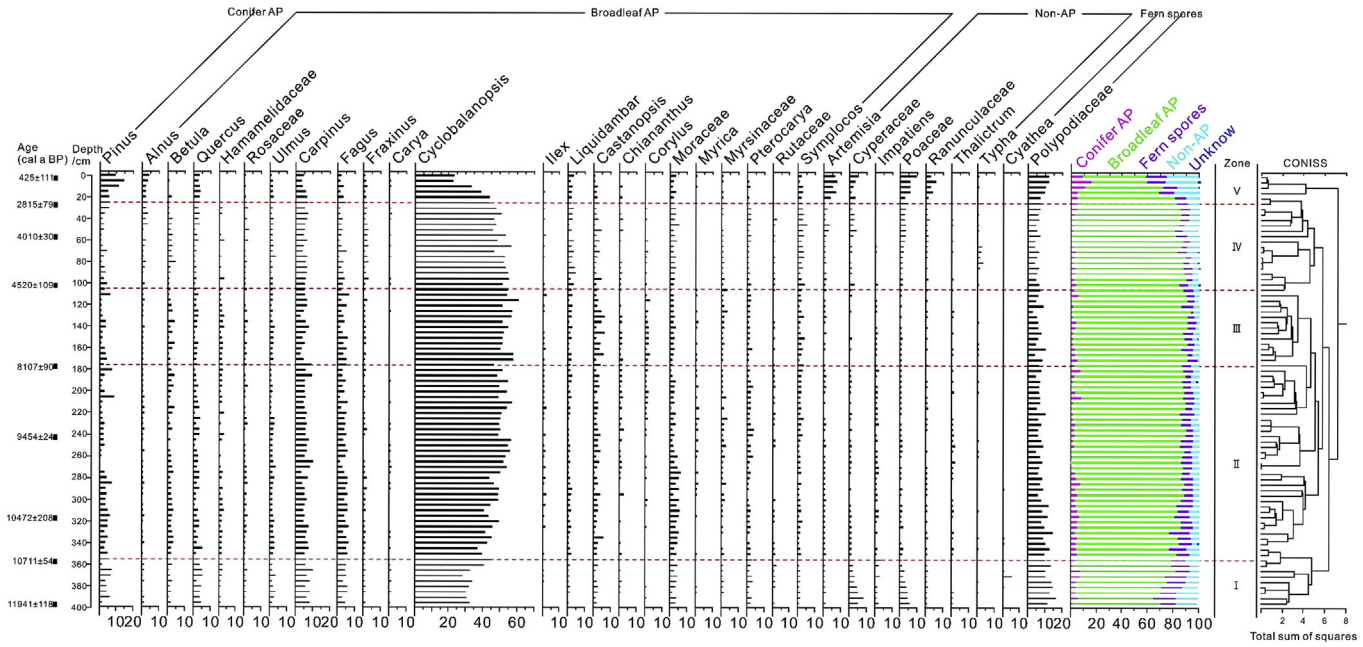


**Fig. 3.** Pollen percentage diagram with zones identified using CONISS software for the core JL15 from Jiulongchi wetland of Fanjing Mountain, SW China.

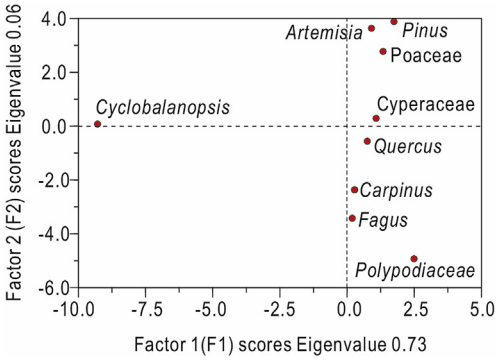


**Fig. 4.** Principal component analysis biplot of major pollen taxa from core JL15 in Fanjing Mountain, SW China.

Erhai lake (Fig. 1) suggested an increasing trend for the evergreen broadleaved trees (*Cyclobalanopsis*, *Lithocarpus* and *Castanopsis*) and *Tsuga* taxa (Shen et al., 2006). These variations of pollen spectrum from southwest China lakes indicated the gradually warming and wetting climate in the early Holocene, which was consistent with our results as recorded in JL15 core from Fanjing Mountain. Our results showed that the temperature increased through 11.9 cal ka BP to 8.0 cal ka BP, and it was the Holocene climatic optimum (HO) during 8.0–4.6 cal ka BP. This record of temperature variation was similar with a previous report about HO during 11.5–6.5 cal ka BP at Huguangyan Maar Lake in south China, approximately 800 km southeast from our study site (Wang et al., 2007, 2016; Zhou et al., 2016).

During 8.0–4.6 cal ka BP (Zone III), the percentage of subtropical AP and subtropical to tropical AP increased up to 54.5% and 15.5%, respectively. The lower percentage of conifer AP and Temperate AP combined with the proxies of AP/T (9.6) and F1 score (−0.6) would suggest a warmer climate. In this period, the decreasing percentages of herb and fern spores and the lower pollen concentration ($93.6 \times 10^3$ grains/g) and sedimentation rate (20 cm $ka^{-1}$) would indicate a warmer and drier climate. Many other lake records in south China showed similar trends. The pollen records of Qinghai crater lake showed that the evergreen broadleaved tree pollens increased, while the deciduous *Quercus* decreased and was gradually replaced by relatively warm local genus of *Alnus* during 8.0–4.6 cal ka BP (Yang et al., 2016). At Chenghai lake, the pollen record indicated a warm period with relatively high proportion of tropical trees during 8.2–4.7 cal ka BP (Xiao et al., 2018). The Tsuga forest coverage continued to increase in 8.2–6.2 cal ka BP at Tiancai lake (Xiao et al., 2014), and the evergreen broadleaved forest and the Tsuga continued to increase in 8.4–6.4 cal ka BP at Erhai lake (Shen et al., 2006). All of these records were in good agreement with our results.

During 4.6–2.6 cal ka BP (Zone IV), the percentages of subtropical AP and subtropical to tropical AP were 51.8% and 14.9%, respectively. The percentage of conifer AP and temperate AP were similar to that in 8.0–4.6 cal ka BP. The proxies of AP/T and F1 scores were 9.1 and −0.3, respectively, which indicate that it was still in the warm period. In this period, the percentage of herb slightly decreased (7.3%) and the fern spores slightly increased (6.0%). The pollen concentration and sedimentation rates were very high with $172.6 \times 10^3$ grains/g and 43.9 cm $ka^{-1}$ respectively. Therefore, the climate would have been relatively warm and wet in this period.

During 2.6 cal ka BP to present (Zone V), the percentage of subtropical AP and subtropical to tropical AP decreased to 34.8% and 10.8%, respectively. However, the percentage of conifer AP and temperate AP increased to 8.8% and 7.8%, respectively. The proxies of AP/T and F1 scores changed to 8.0 and 1.4, respectively. These data would indicate a relatively cool climate. In this period, the percentage of herb and fern spores increased up to 17.2% and 11.7%, respectively. The pollen spectrum in the late Holocene was similar to the period 11.9–10.7 cal ka BP. The pollen concentration ($75.6 \times 10^3$ grains/g) and sedimentation rate (20 cm $ka^{-1}$) were also very low. Therefore, the climate would have been relatively cool and dry in this period. During the late Holocene, the climate gradually changed from warm to relatively cool. However, it was relatively wet in 4.6–2.6 cal ka BP and changed to relatively dry during 2.6 cal ka BP to present. A previous study about pollen records from Chenghai lake sediments also reported that the temperature declined and the precipitation decreased through 4.7 cal ka BP to present in southwest China (Xiao et al., 2018). In the catchment of Qinghai crater lake, it was reported that the hygrophilous species declined after 4.6 cal ka BP (Yang et al., 2016). Pollen evidence from Xingyun lake (Chen et al., 2014), Tiancai lake (Xiao et al., 2014), Lugu lake (Zheng et al., 2014), Haligu lake (Song et al., 2012), and Erhai lake (Shen et al., 2006) generally revealed a gradual decrease in humidity and temperature in southwest China during the late Holocene. Overall, these lake records in Yunnan Province indicated a trend of climate change similar to this study.

Through comparison of pollen records from lake sediments in southwest China (Xiao et al., 2014), north China (Chen et al., 2014),

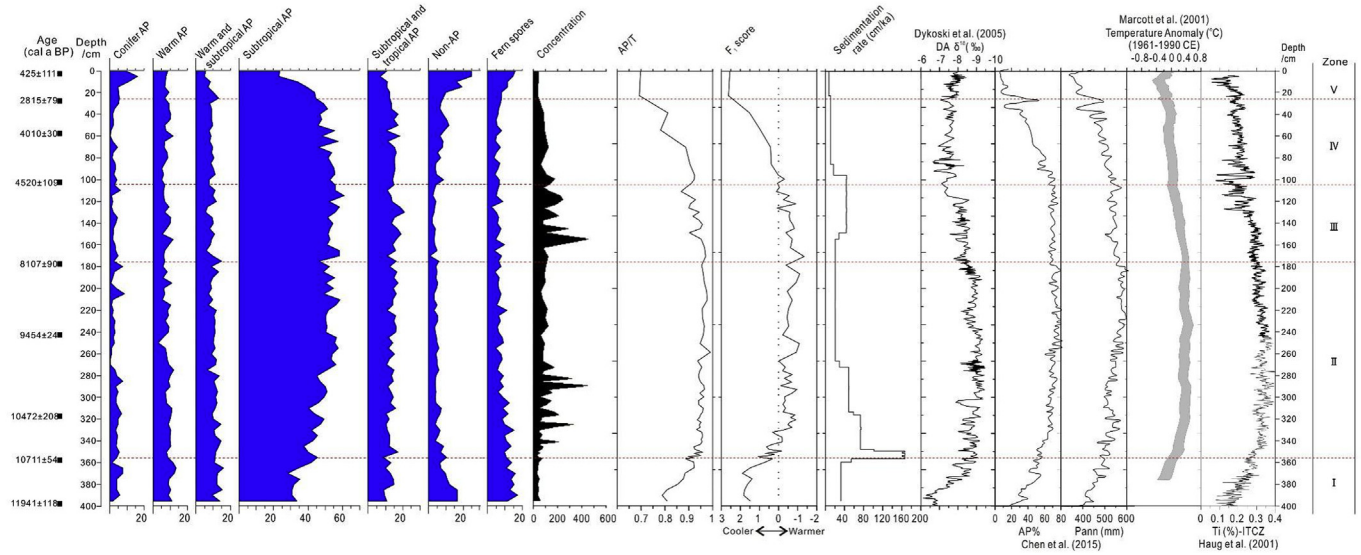


**Fig. 5.** Multiple pollen records from core JL15 in Fanjing Mountain compared with previous records, suggesting asynchronous Holocene precipitation in south and north China.

and south China (this study), the reconstructed Holocene temperature showed synchronous variation, namely, warmer in the early Holocene, warmest in the middle Holocene and cooler in the late Holocene. The general temperature dynamic reflected by our records was similar to the average global temperature anomaly (Marcott et al., 2013). The Holocene temperature change in the EAM area would be mainly controlled by the solar activity, and the temperature change has been supported by pollen evidence from northeast China (Stebich et al., 2015) and the Yangtze delta (Song et al., 2017). Even in the northern North Atlantic, mounting evidence from proxies also suggested that variations in solar activity had played a significant role in controlling Holocene summer sea-surface temperatures (Jiang et al., 2015).

### 5.2. Asynchronous Holocene precipitation in south and north China

According to the pollen records in core JL15 from Fanjing Mountain, the climate in the region was relatively wet in the periods of 10.7–8.0 cal ka BP and 4.6–2.6 cal ka BP, but was the warmest in 8.0–4.6 cal ka BP. This revealed an asynchronization between the precipitation and the temperature. Pollen concentration and sedimentation rate were used as two Holocene precipitation proxies, and they were compared with previous reports of southwest China lakes (Chen et al., 2014; Shen et al., 2006; Song et al., 2012; Xiao et al., 2014; Zheng et al., 2014), which revealed that there was asynchronous Holocene precipitation between south and southwest China. In addition, a comparison of pollen records from the Gonghai lake in the north China and our records (Fig. 4), indicated asynchronous precipitation between south and north China (Chen et al., 2014). However, the Holocene precipitation trend in north China was consistent with that in southwest China, namely, wetter in the early Holocene, the wettest in the middle Holocene, and drier in the late Holocene.

The asynchronous Holocene precipitation was probably due to the impact of EAM in the southwest, north and south China. In the southwest China, the warm and humid climate indicated strong ISM, while cold and dry climate indicated weak ISM (Xiao et al., 2014). The middle Holocene was relatively warm and humid in the southwest China, suggesting a relatively strong ISM in this period. The ISM mainly resulted from seasonal movements of wind belts and the intertropical convergence zone (ITCZ) (Gadgil, 2003; Prive and Plumb, 2007). The precipitation brought by the ISM was relatively sensitive to fluctuations in solar activity, and had relatively high positive correlation with the global temperature anomaly (Marcott et al., 2013) and the north movement of ITCZ (Haug et al., 2001).

However, the Holocene climate in south China was probably not only controlled by ISM. In the EASM areas, previous studies suggested that the monsoon precipitation and insolation-driven temperature changes co-determined the environmental dynamics in north and northeast China (Stebich et al., 2015). In the modern monsoon margin, the climate was co-controlled by prevailing and/or dry westerlies, restricting the northward movement of the subtropical monsoon rainfall belt (An et al., 2012; Stebich et al., 2015; Zhao and Yu, 2012). Therefore, the variation of EASM controlled migration of the monsoon rainfall belt, which was probably a reason for the asynchronous precipitation between the north China and south China in EASM area. With the gradually strengthened EASM from the early to middle Holocene, the precipitation center gradually moved northward, which resulted in a relatively wetter period in south China (10.8–8.0 cal ka BP) and north China (8.0–4.6 cal ka BP). From the early to middle Holocene, this monsoon precipitation gradually transgressed northward, and gradually regressed southward during the late Holocene. This precipitation mechanism had been supported by previous reports (Chu et al., 2014; Chen et al., 2014; Stebich et al., 2015; Xing et al., 2015). Therefore, there would be another relatively wetter period, 4.6–2.6 cal ka BP in the south China.

## 6. Conclusions

A Holocene pollen record from Jiulongchi wetland of Fanjing Mountain in southwest China was reconstructed to understand the climate dynamics. The climate changes during the past 11.8 ka were divided into five stages, mainly characterized by the cold-dry and warm-wet alternation. This was a regional response to the Asian monsoon changes in the context of past global changes in the Holocene. The asynchronous Holocene precipitation was observed in the south, north and southwest China through comparison of multiple pollen records, which was probably triggered mainly by the different monsoons. In EASM area, the monsoon precipitation gradually transgressed northward during the early Holocene to middle Holocene and then regressed southward during the late Holocene, which led to another relatively wetter period, 4.6–2.6 cal ka BP in the south China.

## Acknowledgments

This research was jointly supported by the National Top Discipline Construction Project of Guizhou Province (85 2017 Qianjiao Keyan Fa), the Project of Innovation Program for Postgraduate Education of Guizhou Province (04 2016 Qianjiao Yanhe GZS Zi), the NSFC-Belmont Forum Joint Research Project (No. 4166114404), Scientific Research Foundation for Doctor of Guizhou Normal University (No. 119040516016), the Provincial Program on Science and Technology of Guizhou Province (7198 2016 Qiankehe LH), and Science Foundation for Doctorate Research of Guizhou Normal University (2016). We also thank Dr. Neil McLaughlin (Agriculture and Agri-Food Canada) for his excellent language polishing.

## Appendix A. Supplementary data

Supplementary data to this article can be found online at https://doi.org/10.1016/j.quaint.2019.01.009.

## References

An, Z., Colman, S.M., Zhou, W., Li, X., Brown, E., Jull, A.T., Cai, Y., Huang, Y., Lu, X., Chang, H., Song, Y., Sun, Y., Xu, H., Liu, W., Jin, Z., Liu, X., Cheng, P., Liu, Y., Li, A., Li, X., Liu, X., Yan, L., Shi, Z., Wang, X., Wu, F., Qiang, X., Dong, J., Lu, F., Xu, X., 2012. Interplay between the westerlies and Asian monsoon recorded in Lake Qinghai sediments since 32 ka. Sci. Rep. 2, 619.

An, Z., Porter, S.C., Kutzbach, J.E., Wu, X., Wang, S., Liu, X., Li, X., Zhou, W., 2000. Asynchronous Holocene optimum of the east asian monsoon. Quat. Sci. Rev. 19 (8), 743–762.

Blaauw, M., 2010. Methods and code for 'classical' age-modelling of radiocarbon sequences. Quat. Geochronol. 5 (5), 512–518.

Chen, F., Chen, X., Chen, J., Zhou, A., Wu, D., Tang, L., Zhang, X., Huang, X., Yu, J., 2014. Holocene vegetation history, precipitation changes and Indian summer monsoon evolution documented from sediments of Xingyun Lake, South-West China. J. Quat. Sci. 29 (7), 661–674.

Chu, G., Sun, Q., Xie, M., Lin, Y., Shang, W., Zhu, Q., Shan, Y., Xu, D., Rioual, P., Wang, L., Liu, J., 2014. Holocene cyclic climatic variations and the role of the Pacific Ocean as recorded in varied sediments from North-eastern China. Quat. Sci. Rev. 102, 85–95.

Dykoski, C.A., Edwards, R.L., Cheng, H., Yuan, D., Cai, Y., Zhang, M., Lin, Y., Qing, J., An, Z., Revenaugh, J., 2005. A high-resolution, absolute-dated Holocene and deglacial Asian monsoon record from Dongge cave, China. Earth Planet. Sci. Lett. 233 (1–2), 71–86.

Etienne, D., Ruffaldi, P., Dupouey, J.L., Georges-Leroy, M., Ritz, F., Dambrine, E., 2013. Searching for ancient forests: a 2000 year history of land use in northeastern French forests deduced from the pollen compositions of closed depressions. Holocene 23 (5), 678–691.

Faegri, K., Iversen, J., 1989. Textbook of Pollen Analysis, fourth ed. Knut Faegri, Peter Emil Kaland and Knut Krzywinski, John Wiley & Sons, Chichester, pp. 328.

Gadgil, S., 2003. The Indian monsoon and its variability. Annu. Rev. Earth Planet Sci. 31 (1), 429–467.

Grimm, E., 2011. Tilia and Tiliagraph Software 1.7.16. Illinois State Museum, Springfield.

Haug, G.H., Hughen, K.A., Sigman, D.M., Peterson, L.C., Röhl, U., 2001. Southward migration of the intertropical convergence zone through the Holocene. Science 293, 1304–1308.

Jia, G., Bai, Y., Yang, X., Xie, L., Wei, G., Ouyang, T., Chu, G., Liu, Z., Peng, P., 2015. Biogeochemical evidence of Holocene East Asian summer and winter monsoon variability from a tropical maar lake in southern China. Quat. Sci. Rev. 111, 51–61.

Jiang, H., Muscheler, R., Björck, S., Seidenkrantz, M.S., Olsen, J., Sha, L., Sjolte, J.,

Eiríksson, J., Ran, L., Knudsen, K.L., Knudsen, M.F., 2015. Solar forcing of Holocene summer sea-surface temperatures in the northern North Atlantic. Geology 43 (3), 203–206.
Mackenzie, L., Bao, K., Mao, L., Klamt, A.M., Pratte, S., Shen, J., 2018. Anthropogenic and climate-driven environmental change in the Songnen Plain of northeastern China over the past 200 years. Palaeogeogr. Palaeoclimatol. Palaeoecol. 511, 208–217.
Marcott, S.A., Shakun, J.D., Clark, P.U., Mix, A.C., 2013. A reconstruction of regional and global temperature for the past 11,300 years. Science 339 (6124), 1198–1201.
Panigrahi, G., Patnaik, S., 1961. Cytology of some genera of Polypodiaceae in eastern India. Nature 191, 1207–1208.
Park, J., Shin, Y.H., Byrne, R., 2016. Late-Holocene vegetation and climate change in Jeju Island, Korea and its implications for ENSO influences. Quat. Sci. Rev. 153, 40–50.
Prive, N., Plumb, R., 2007. Monsoon dynamics with interactive forcing. Part I: axisymmetric studies. J. Atmos. Sci. 64, 1417–1430.
Ran, M., Feng, Z., 2013. Holocene moisture variations across China and driving mechanisms: a synthesis of climatic records. Quat. Int. 313, 179–193.
Reimer, P.J., Bard, E., Bayliss, A., Beck, J.W., Blackwell, P.G., Ramsey, C.B., Buck, C.E., Cheng, H., Edwards, R.L., Friedrich, M., Grootes, P., Guilderson, T.P., Haflidason, H., Hajdas, I., Hatte, C., Heaton, T., Hoffmann, D.L., Hogg, A.G., Hughen, K.A., Kaiser, K.F., Kromer, B., Manning, S.W., Niu, M., Reimer, R.W., Richards, D.A., Scott, E.M., Southon, J.R., Staff, R., Turney, C., Plicht, J., 2013. IntCal13 and marine13 radiocarbon age calibration curves 0-50,000 years cal BP. Radiocarbon 55 (4), 1869–1887.
Shen, J., Jones, R.T., Yang, X., Dearing, J.A., Wang, S., 2006. The Holocene vegetation history of Lake Erhai, Yunnan province southwestern China: the role of climate and human forcings. Holocene 16 (2), 265–276.
Sheng, M., Wang, X., Zhang, S., Chu, G., Su, Y., Yang, Z., 2017. A 20,000-year high-resolution pollen record from Huguangyan Maar Lake in tropical-subtropical South China. Palaeogeogr. Palaeoclimatol. Palaeoecol. 472, 83–92.
Song, B., Li, Z., Lu, H., Mao, L., Saito, Y., Yi, S., Lim, J., Li, Z., Lu, A., Sha, L., Zhou, R., Zuo, X., Pospelova, V., 2017. Pollen record of the centennial climate changes during 9-7 cal ka BP in the Changjiang (Yangtze) River Delta plain, China. Quat. Res. 87 (2), 275–287.
Song, X., Yao, Y., Wortley, A.H., Paudayal, K.N., Yang, S., Li, C., Blackmore, S., 2012. Holocene vegetation and climate history at Haligu on the jade dragon snow mountain, yunnan, SW China. Climatic Change 113, 841–866.
Stebich, M., Rehfeld, K., Schlütz, F., Tarasov, P.E., Liu, J., Mingram, J., 2015. Holocene vegetation and climate dynamics of NE China based on the pollen record from Sihailongwan Maar Lake. Quat. Sci. Rev. 124, 275–289.
Su, J., Zhang, Y., Dong, S., Chen, X., Li, Y., Cui, J., 2014. Geochronology and Hf isotopes of granite gravel from fanjingshan, south China: implication for the precambrian tectonic evolution of western jiangnan orogen. J. Earth Sci. 25 (4), 619–629.
Wang, S., Lü, H., Liu, J., Negendank, J., 2007. The early Holocene optimum inferred from a high-resolution pollen record of Huangyan Maar Lake in southern China. Chin. Sci. Bull. 52 (20), 2829–2836.
Wang, X., Chu, G., Sheng, M., Zhang, S., Li, J., Chen, Y., Tang, L., Su, Y., Pei, J., Yang, Z., 2016. Millennial-scale Asian summer monsoon variations in South China since the last deglaciation. Earth Planet. Sci. Lett. 451, 22–30.
Wang, Y., Cheng, H., Edwards, R.L., He, Y., Kong, X., An, Z., Wu, J., Kelly, J.M., Dykoski, A.C., Li, X., 2005. The Holocene Asian monsoon: links to solar changes and north Atlantic climate. Science 308 (5723), 854–857.
Wang, Y., Liu, X., Herzschuh, U., 2010. Asynchronous evolution of the Indian and East Asian summer monsoon indicated by Holocene moisture patterns in monsoonal central asia. Earth Sci. Rev. 103 (3), 135–153.
Wu, X., Zhang, Z., Xu, X., Shen, J., 2012. Asian summer monsoonal variations during the Holocene revealed by Huguangyan maar lake sediment record. Palaeogeogr. Palaeoclimatol. Palaeoecol. 323, 13–21.
Xiao, X., Haberle, S., Li, Y., Liu, E., Shen, J., Zhang, E., Yin, J., Wang, S., 2018. Evidence of Holocene climatic change and human impact in northwestern Yunnan Province: high-resolution pollen and charcoal records from Chenghai Lake, southwestern China. Holocene 28 (1), 127–139.
Xiao, X., Haberle, S.G., Shen, J., Yang, X., Han, Y., Zhang, E., Wang, S., 2014. Latest Pleistocene and Holocene vegetation and climate history inferred from an alpine lacustrine record, northwestern Yunnan Province, southwestern China. Quat. Sci. Rev. 86, 35–48.
Xing, W., Bao, K., Gallego-Sala, A.V., Charman, D.J., Zhang, Z., Gao, C., Lu, X., Wang, G., 2015. Climate controls on carbon accumulation in peatlands of Northeast China. Quat. Sci. Rev. 115 (9), 78–88.
Xu, D., Lu, H., Wu, N., Liu, Z., Li, T., Shen, C., Wang, L., 2013. Asynchronous marine-terrestrial signals of the last deglacial warming in East Asia associated with low- and high-latitude climate changes. Proc. Natl. Acad. Sci. Unit. States Am. 110 (24), 9657–9662.
Yang, Y., Zhang, H., Chang, F., Meng, H., Pan, A., Zheng, Z., Xiang, R., 2016. Vegetation and climate history inferred from a Qinghai crater lake pollen record from Tengchong, southwestern China. Palaeogeogr. Palaeoclimatol. Palaeoecol. 461, 1–11.
Zhao, Y., Yu, Z., 2012. Vegetation response to Holocene climate change in East Asian monsoon-margin region. Earth Sci. Rev. 113 (1), 1–10.
Zheng, Q., Zhang, H., Ming, Q., Chang, F., Meng, H., Zhang, W., Liu, M., Shen, C., 2014. Vegetational and environmental changes since 15 ka BP recorded by Lake Lugu in the southwest monsoon domain region. Quat. Sci. 34, 1314–1326 (in Chinese with English abstract).
Zhou, X., Sun, L., Zhan, T., Huang, W., Zhou, X., Hao, Q., Wang, Y., He, X., Zhao, C., Zhang, J., Qiao, Y., Ge, J., Yan, P., Yan, Q., Shao, D., Chu, Z., Yang, W., Smol, J.P., 2016. Time-transgressive onset of the Holocene optimum in the east asian monsoon region. Earth Planet. Sci. Lett. 456, 39–46.